



Indoor-outdoor NO_x modelling in a single-side naturally ventilated room in a real building in Madrid

E. Rivas^{a,e,*}, J.L. Santiago^a, F. Martín^a, A. Martilli^a, E. Díaz^a, F.J. Gómez-Moreno^a, B. Artiñano^a, C. Román-Cascón^b, C. Yagüe^c, D. de la Paz^d, R. Borge^d

^a Environmental Department, CIEMAT, Avenida Complutense 40, 28040, Madrid, Spain

^b Applied Physics Department, University of Cádiz, INMAR, Puerto Real, 11510, Spain

^c Departamento de Física de la Tierra y Astrofísica, Universidad Complutense de Madrid (UCM), Plaza Ciencias 1, 28040, Madrid, Spain

^d Department of Chemical and Environmental Engineering, Universidad Politécnica de Madrid (UPM), Calle José Gutiérrez Abascal 2, 28006, Madrid, Spain

^e Vicerrectorado de Investigación, Innovación y Doctorado, Universidad Politécnica de Madrid (UPM), Ramiro de Maeztu 7, 28040, Madrid, Spain

ARTICLE INFO

Keywords:

Computational Fluid Dynamics (CFD)
NO_x traffic emissions
Indoor Air Quality (IAQ)
Single-Sided Ventilation (SSV)
Air pollution and health

ABSTRACT

The specific objectives of this work are to assess a Computational Fluid Dynamics (CFD) modelling performance through data of one experimental campaign, to quantify the impact of outdoor NO_x traffic emissions on indoor NO_x concentration and to investigate the natural ventilation using the infiltrated NO_x concentration decay and the Air Changes per Hour (ACHs). For this purpose, NO_x transport phenomena in a single-side naturally ventilated room in a real building in Madrid is investigated through an Unsteady Reynolds-Averaged Navier-Stokes (URANS) approach and individual passive scalar transport equations for each source (parked vehicles with the engine idling, street traffic and urban background). The combination of this methodology with suitable boundary conditions properly reproduces the time evolution of Wind Speed (WS), Wind Direction (WD) and Turbulent Kinetic Energy (κ), both inside the streets and above the buildings, even for $WS < 1 \text{ m s}^{-1}$, and also outdoor and indoor NO_x concentrations. In this case, urban background significantly contributes to the indoor concentration and idling vehicles just below the room can contribute between 10 % and 50 % to the total indoor concentration, even when their emissions are considerably smaller than those of traffic in nearby streets. The Indoor-Outdoor NO_x concentration ratio (I/O) depends not only on the outdoor concentration (which, at the same time, depends on the atmospheric turbulence) but also on the ventilation (in this case, type Single-Sided Ventilation, SSV), showing a wide range of values. The impact of an indoor Heat Source (HS) below the open window on I/O is low, but under certain meteorological conditions, the stack pressure could be more important than the wind pressure. The time required to ventilate the room is 3.4 min. It has been obtained using the infiltrated NO_x concentration decay and has been verified through the average ACH, $\langle ACH(t) \rangle$.

These results provide a better understanding of the impact of the meteorological conditions in outdoor-indoor NO_x exchange by natural ventilation, which is the main goal of this research.

* Corresponding author. Environmental Department, CIEMAT, Avenida Complutense 40, 28040, Madrid, Spain.

E-mail addresses: esther.rivas.ramos@upm.es, esther.rivas@externos.ciemat.es (E. Rivas).

<https://doi.org/10.1016/j.job.2023.108403>

Received 24 September 2023; Received in revised form 13 December 2023; Accepted 26 December 2023

Available online 29 December 2023

2352-7102/© 2024 The Authors.

Published by Elsevier Ltd. This is an open access article under the CC BY license

(<http://creativecommons.org/licenses/by/4.0/>).

1. Introduction

Air pollution is one of the most influential factors on human health [1]. According to the WHO, the diseases most closely associated with exposure to air pollution are stroke, ischemic heart disease, chronic obstructive pulmonary disease, lung cancer, pneumonia, and cataracts [2]. In addition, the risk of suffering, among other, diseases such as some types of cancer, diabetes, cognitive decline, neurological diseases and premature births, is linked to exposure to air pollution [2]. Typical air pollutants regulated according to health-based criteria are NO₂ and PM [3]. While worldwide mortality is mainly associated to PM_{2.5} [4], NO₂ is major concern in urban areas where traffic emissions concentrate and has been identified as a key pollutant to prevent air pollution-related premature mortality in Madrid [5], where this study takes place.

Consistently with the relative risks derived from epidemiological studies [6], pollutant concentrations data from air quality monitoring stations are commonly used to estimate the health impacts [7]. However, it is well known that their spatial representativeness is limited in urban environments, where most people live [8–10]. This is due to the combination of certain meteorological conditions and urban morphologies that induces complex flow patterns inside the streets [11]. This fact, together with traffic roads, which is the main source of elevated NO₂ levels in EU cities [12], can give rise to very heterogeneous spatial distributions of NO₂ in the same street, with elevated maximum values at pedestrian height [13–16]. In addition, indoor exposure is not usually considered, and people spends more than 90 % of their time indoors: homes, workplaces, public spaces, etc. [17]. For this reason, it is important to account for those microenvironments in the assessment of total exposure to airborne pollutants. Hence, recent measuring and modelling efforts have been done to take into account the complexity of urban areas and indoor exposure. In this context, CFD models can be a very interesting tool for this purpose.

To determine gradients of concentration in urban areas, extensive field campaigns and/or numerical simulations at high spatial resolution are needed. Experimental campaigns usually focus on urban hotspots and cover areas up to 1 km². Highly detailed concentration maps corresponding to the sampling period of, at least, one week can be obtained by means of a dense distribution of passive samplers' deployment throughout the studied area [14]. Similarly, high spatial resolution can be achieved by means of CFD models. The increasing of computational resources is making affordable covering larger study areas, up to 10 km² [18] and simulating larger periods. Therefore, CFD simulations can add valuable information to experimental campaigns and/or urban air quality monitoring stations [19]. These high spatial resolution pollutant concentration distributions are used to obtain more accurate estimates of exposure [18] and even these maps were combined with pedestrian mobility microsimulations to estimate pedestrian exposure at urban pollution hotspots [20]. CFD models can also consistently describe the link between outdoor and indoor air quality [21]. However, modelling indoor environments requires considering specific factors such as ventilation. Ventilation rates have been associated to health outcomes although more research is needed to substantiate the causality of this association [22].

Ventilation can be made by means of natural, mechanical or hybrid, and/or purification techniques [23]. Natural ventilation is the simplest and cheapest option to renew indoor air. It consists of inducing an airflow between outdoors and indoors by opening windows, doors, ventilation grills or any other opening placed in the building envelope. Induced flow is due to outdoor-indoor pressure differences generated by the wind effect, by outdoor-indoor temperature differences or both. Hence, the main two handicaps of natural ventilation are its strong dependence on meteorological conditions and its potential contribution to increase indoor exposure due outdoor pollution entrainment.

Few CFD studies considering the natural ventilation of indoor environments have been found in the literature. Tong et al [24] studied the impact of various building parameters on the indoor air quality of a naturally ventilated building in a near-road environment using a CFD model. However, they considered an isolated building and neglected the stack pressure effect. Yang et al [25] and Mohammadi & Calautit [26] analysed the traffic-induced pollution on indoor air quality depending on the season and the natural ventilation strategy, respectively. Both studies used CFD models but neglecting the influence of buildings around the street canyon and the stack pressure effect. Xiong and Chen [27] investigated the effects of horizontal sunshields on the pollutant dispersion and indoor air quality of windward rooms by Single-Sided Ventilation (SSV), considering isothermal and non-isothermal boundary conditions along an idealized street canyon. SSV occurs when all openings are on a same facade, regardless of the opening number and position [28] and is commonly classified according to the opening number, i.e. SS1 (Single-Sided with 1 opening) and SSn (Single-Sided with multiple (n) openings). In SS1, the air enters and leaves the indoor environment through the same opening [29]. Hu et al. [30] studied the impacts of outdoor-indoor air temperature differences considering different natural ventilation schemes on traffic-related pollutant dispersion in an idealized street canyon by means of CFD modelling. Santiago et al. [21] investigated the Indoor-Outdoor concentration ratio (I/O) for traffic-related pollutants in a naturally ventilated building located in an idealized urban environment as a function of the wind direction and the configuration of open and closed windows using CFD modelling, but only considering the wind effect. Hence, to gain confidence in CFD models, it is necessary to assess their performance on real urban environments considering both the wind effect and outdoor-indoor air temperature differences, as already pointed out by Ai & Mak [31].

In this context, this study presents a comprehensive assessment of urban air quality modelling including an indoor environment. A CFD model is applied to a virtual twin of the *San Carlos* Hospital building (Madrid, Spain) and its surroundings, where different experimental campaigns were carried out in the framework of the AIRTEC-CM Project (<https://airtec-cm.es/>) with three main goals:

1. To assess the CFD modelling performance through data of one experimental campaign
2. To quantify the impact of outdoor NO_x traffic emissions on indoor NO_x concentration
3. To investigate the natural ventilation using the infiltrated NO_x concentration decay and the ACHs

The novelties of this work are the following:

- The numerical domain, which cover even the Hospital indoor environment, consistently bridging the gap between outdoor and indoor simulation
- The model, which explicitly simulates the wind effect and outdoor-indoor temperature differences when natural ventilation starts using an URANS approach. Outdoor-indoor temperature gradients are not typically included in these studies
- NO_x emissions are simulated using individual passive scalar transport equations for each source, allowing to address goals 2 and 3 simultaneously and independently
- The time evolution of modelled NO_x concentration both indoor and outdoor are evaluated during a winter day, when the indoor environment was naturally ventilated through an open window, SS1. This kind of evaluation has not been reported previously in the bibliography

The manuscript is structured as follows: in the “Material and methods” section the study area, observational datasets, traffic emissions, and CFD model are described. “Results and discussion” are presented in Section 3, including mesh sensitivity test (§ 3.1), meteorology (§ 3.2) and air quality (§ 3.3). Resulting outdoor-indoor NO_x concentrations are discussed, considering the effects of urban background, local emissions and an indoor HS. The SSV is analysed using the infiltrated NO_x concentration decay and the ACHs. Finally, the main conclusions from the study are drawn in § 4.

2. Material and methods

2.1. Study area, experimental campaign and emissions

The study area focuses on the *San Carlos Hospital*, located in the *Ciudad Universitaria* neighbourhood in the western area of Madrid City. The hospital is surrounded by high-rise buildings (the height of the tallest building, z_{max} , is 47 m) and streets with intense traffic (Figure SM1 a) in the east. Most of the streets in this area are two-way roads with several lanes. The vegetation around the hospital (mostly trees) is deciduous, so in wintertime its effects on air quality can be considered negligible [32].

Different experimental campaigns were carried out to record meteorological and air pollutant measurements in the surroundings of the *San Carlos Hospital*, as well as in a room located on the fourth floor of one of the corners of the hospital’s east wing (Fig. 1). This room represent the indoor environment. The room, which dimensions are $7.5 \times 5 \times 3 \text{ m}^3$, has an access door and two windows facing northeast, whose dimensions are $2 \times 1 \text{ m}^2$ (Fig. 1).

Measurements were made during the winter, when some episodes of high NO₂ pollution are observed in Madrid [33], and are summarized in Table 1. The simulation of this study corresponds to February 18, 2021, a weekday characterized by a typical traffic pattern with peaks between 7 and 10 LST, 13–16 LST, and 17–20 LST. The test was carried out without any person in the room and is divided into two phases from the IAQ point of view:

1. from 4:00 LST to 8:40 LST, when both windows were closed. Therefore, inside the room the increasing of pollutant concentration is due to infiltration
2. from 8:40 LST to 14:00 LST, when one window remained closed, but the other window was completely opened. Therefore, inside the room the increasing of pollutant concentration is due to SS1

This test has been chosen because it covers a wide range of working conditions, both meteorological variables and NO_x traffic emissions. The variability helps guarantee the reliability and repeatability of the simulation.

During the test, on the one hand, 1 min resolution NO₂ and NO concentrations were measured indoor and outdoor using two Thermo Scientific™ monitors model 42i and 42iTL (noted as AQ MS ROOM and AQ MS WINDOW, respectively in Fig. 1): at 2 m from the open window inwards (IN point, Fig. 1) and outwards (OUT point, Fig. 1). In addition, the indoor air temperature was measured



Fig. 1. Right) *San Carlos Hospital* (Madrid): outdoor view. Left up) Location of some ambulances. Left down) room: indoor view. Measurements location (red points). (Source: Google Earth satellite image).

Table 1
Summary of the experimental data. All variables were consistently synchronized over 10 min periods.

Location		Study Area				
Environment		Inside				Outside
		Indoor	Outdoor			Outdoor
Measuring Point		IN	OUT	ROOF	GROUND	TOWER
Data	Meteorological	T	--	WS, WD, T, κ	WS, WD	WS, WD, T_u , T_d
	Air quality	NO, NO ₂	NO, NO ₂	---	NO, NO ₂	---

with a 1 min resolution using a Grimm model EDM 365 equipped with a temperature probe EE08. This study focuses on NO_x concentrations for minimizing the effects of atmospheric chemistry (NO_x concentrations are computed from NO and NO₂ concentrations and express as NO₂ mass). More detailed information about air quality instruments at the *San Carlos* Hospital room during experimental campaigns can be found in Alonso-Blanco et al. [34] since a similar deployment was used.

On the other hand, WS, WD and air temperature (T) were measured using a portable Campbell Scientific® weather station (noted as Met. MS ROOF in Fig. 1) on the hospital roof, 34 m above the base of the building (ROOF point, Fig. 1). These data were subsequently averaged into 10 min data means. The κ was derived from high-frequency measurements of the three components of the flow obtained from a sonic anemometer IRGASON®. Besides, NO₂ and NO concentrations were recorded 50 m east from the corner at the street level (GROUND point, Fig. 1), as well as WS and WD. These data measured using a mobile air quality monitoring station equipped with a portable weather station from the Madrid City Council (noted as AQ MS GROUND + Met. MS GROUND in Fig. 1) were also averaged in 10 min.

In addition, from a meteorological tower located 2 km northward from the study area (TOWER point, Figure SM1 b) WS, WD and T at 54.29 m and T at 3.6 m Above Ground Level, AGL, (T_u and T_d respectively) were measured using RM-Young sensors model 5305LM-59 and 41382LC respectively (noted as Met. S. TOWER in Figure SM1 b) to characterize inlet conditions and atmospheric thermal

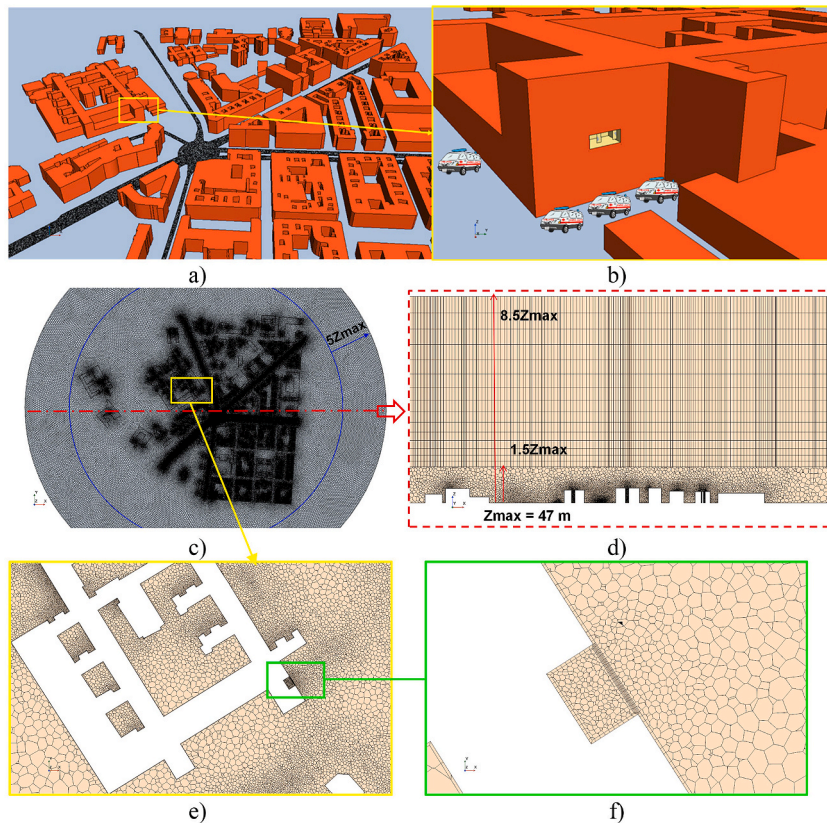


Fig. 2. a) Geometric model of buildings (in red) and roads network (in black). b) Zoom of the *San Carlos* Hospital and the room where the experimental campaign was carried out including the recreation of ambulance locations. c) mesh view in a horizontal plane section (at 3 m height); d) mesh view in a vertical plane section; e) mesh view in a horizontal plane section (at 14 m height, corresponding to the fourth floor of the Hospital); f) mesh zoom around the room.

stability for simulations. These data were recorded every 10 min.

In this study, only traffic emissions were considered. Hourly NO_x emissions were estimated in all the streets around the Hospital (Figure SM1 a) following the methodology described by Borge et al. [35]. The road network in the modelling domain includes 384 links, corresponding to 27.2 km of single lane total length. Hourly fluxes were derived from a regional traffic demand model, calibrated specifically for February 18, 2021 with traffic counts available at Isaac Peral St., adjacent to the Hospital, yielding a total mileage of 215943 veh-km for that day. Emissions factors were derived from COPERT [36] version 5.0, considering hourly-specific average speed in each link and the fleet composition corresponding to that area of Madrid according to Pérez et al. [37]. As a result, a total estimate of 97 kg NO_x was obtained for the completely traffic-modelling domain. For the sake of simplicity, in CFD-modelling domain only the most crowded streets around the Hospital are considered (as time-variable emissions $E_{C_i}(t)$, being i each entire street, see § 2.2.2). Details on the temporal and spatial emissions breakdown can be found in the supplementary material, Figures SM2 and SM3 respectively.

Arriving ambulances usually park around the hospital (Fig. 1) and stay there idling for long periods. Due to this fact, one parked ambulance in front of the emergency entrance (hospital south wing), and three parked ambulances on this corner, just below the room (Fig. 2 b) are considered in numerical simulations. Since COPERT does not include vehicle idle emission factors, we considered some moving/idling emission ratios from the literature [38,39] and applied it to Euro 5 light duty diesel vehicles, which may represent the average characteristics of ambulances. As a result, time-constant emissions, $A_{C_i} = 5 \text{ g h}^{-1}$, being i each ambulance, are imposed assuming they are parked with the engine idling. This corresponds to a total aggregated NO_x emission of approximately 0.5 kg over the day.

2.2. CFD model

2.2.1. Computational domain and mesh

A 3D model in an area of approximately 2.5 km² around the *San Carlos* Hospital has been built based on the blocks municipal cartography from Madrid City Council including building height from LiDAR measurements. Subsequently, the hospital building was edited to include the specific room included in the study. The traffic emission region is that shown in dashed yellow line in Figure SM1. For modelling purposes, cars emissions are vertically distributed in the first meter above ground level (Fig. 2 a).

Top boundary is approximately 8.5 Z_{\max} height and distance from buildings up to the inlet boundary (>8 times the building heights) has been established according to the best practice guidelines [40,41].

The mesh model used is a combination of polyhedral cells whose maximum size, ΔV_{\max} , is 100 m³ up to 1.5 Z_{\max} and 15 layers of prismatic cells from 1.5 Z_{\max} up to 8.5 Z_{\max} (top of urban atmosphere) whose size grows hyperbolically with height (Fig. 2 d). The polyhedral mesh has been refined both around buildings and around roundabout and radial traffic roads (Fig. 2 c) in such a way that:

1. On surfaces (ground and buildings), cells have a maximum size, ΔS_{\max} , of 100 m² and a minimum size, ΔS_{\min} , of 0.5 m² (see mesh sensitivity test, § 3.1) and, a thickness of 0.25 m (equivalent to a prismatic layer, PL)
2. Cells grow very slowly from surfaces to the bulk (surface growth rate is 1.1, Fig. 2 e)
3. There are at least 8 cells per street

In addition, to adequately capture air changes through the opened window during the experiment, the PLs at both sides of the outdoor-indoor interface have been divided into 3 sublayers (see mesh sensitivity test, § 3.1 and Fig. 2 f). This mesh model has been chosen according to the mesh test carried out (see mesh sensitivity test, § 3.1).

For meshing, the automatic tool of STAR-CCM+16.02.009-R8® [42] has been used.

2.2.2. Model description and simulation set-up

The model is based on Unsteady Reynolds-averaged Navier-Stokes (URANS) equations considering the Realizable $k - \epsilon$ Two-Layer closure [43]. This approach is considered a good compromise between accuracy and computational cost and their use is widespread in simulations of atmospheric pollutant dispersion in urban environments [21,25,44]. The air is assumed as an ideal gas with constant properties and the gravity is considered.

Traffic-related NO_x dispersion is simulated as a non-reactive pollutant using passive scalar transport equations (Eq. 1). In order to estimate the contribution of each emission source (entire streets and ambulances) on final concentration, one passive scalar corresponding to each contribution is simulated (12 streets and 4 ambulances, see § 2.1). Total NO_x concentration is the sum of concentrations of each contribution. For each i^{th} source:

$$\left\{ \partial_t C_i(\vec{r}, t) + \partial_{x_j} \left(\rho u_j C_i(\vec{r}, t) - \frac{\mu_t}{Sc_t} \partial_{x_j} C_i(\vec{r}, t) \right) = E_{C_i}(t) \text{ or } A_{C_i} \right\}_{j=x,y,z} \quad (\text{Eq. 1})$$

where $C_i(\vec{r}, t)$ is the NO_x concentration at location \vec{r} and time t from i^{th} pollutant source, ρ is the air density, u_j the j -component of flow, μ_t is the turbulent viscosity, Sc_t is the turbulent Schmidt number and $E_{C_i}(t)$ and A_{C_i} are the NO_x emitted by each i^{th} entire street at time t or each i^{th} ambulance respectively. Sc_t is assumed equal to 0.7 [45–47] and $E_{C_i}(t)$ data are updated each hour. Simulations are performed with a time step, Δt , of 1 s and 1 inner iteration per Δt , except between 8:40 LST and 9 LST, where 10 inner iteration per Δt are used to accurately capture the sudden change in outdoor-indoor, and vice-versa, NO_x exchange when the window is open. It is verified that simulations are time-step independent and the CFL was of the order of 1 both indoor and in most of the outdoor.

Symmetric boundary conditions are imposed at the top of the domain. The ground is considered a rough wall with $z_0 = 0.03$ m and buildings as smooth walls. Both are adiabatic surfaces. The All Y+ wall treatment is used [43].

At inlet boundary, neutral vertical profiles for the wind speed, $u(z, t)$ (Eq. 2), turbulent kinetic energy, $k(t)$ (Eq. 3), and dissipation rate, $\varepsilon(z, t)$ (Eq. 4) are imposed [48].

$$u(z, t) = \frac{u^*(t)}{k} \ln \left\{ \frac{z + z_0}{z_0} \right\} ; \quad (\text{Eq. 2})$$

$$k(t) = \frac{u^*(t)^2}{\sqrt{C_\mu}} ; \quad (\text{Eq. 3})$$

$$\varepsilon(z, t) = \frac{u^*(t)^3}{k(z + z_0)}, \quad (\text{Eq. 4})$$

where $u^*(t)$ is the friction velocity, z_0 is the roughness length, C_μ is a model constant ($C_\mu = 0.09$) and k is von Karman's constant ($k = 0.4$). WS and WD are taken from the meteorological tower (Met. S. TOWER, Figure SM1 b), Fig. 3. In order to take into account the stack pressure effect, the temperature above the Hospital, at the ROOF point, at 8:40 LST (just when the window is open), is imposed at inlet ($T_{out} = 281$ K) and the initial indoor temperature is established as the indoor temperature at 8:40 LST ($T_{in} = 298$ K).

For NO_x urban background contribution, a uniform profile, $UB_{C_i}(t)$, is imposed at inlet with concentration changing every 10 min corresponding from some fixed urban background AQMS near the district from the Madrid City Council (see supplementary material, Figure SM4). Note that measurements from several urban AQMS are used to study the impact of using different urban background concentrations. Using individual passive scalar transport equations for district and ambulances NO_x emissions, $E_{C_i}(t)$ and A_{C_i} , respectively and NO_x urban background, $UB_{C_i}(t)$, allows quantifying the influence of each outdoor source on indoor NO_x concentration.

Since heating could influence the outdoor-indoor temperature differences (i.e., the stack pressure effect), a 1500 W heater (typical thermal power for a 40 m² room with two windows) installed just below the open window is simulated. In this way, the room ventilation due to outdoor-indoor temperature gradient is simulated. Note that, only convection heat transfer between heater and air is simulated and no external thermal loads are considered.

Some common indoor pollutants can be biological, especially in hospital environments, for example, viruses transmitted by people. Natural ventilation also dilutes and removes the indoor pollutants by providing fresh air. In fact, improving natural ventilation in shared indoor/semi-indoor environments is recommended as infectious agents' exposure reduction measure [49,50]. However, measuring natural ventilation in real conditions is complicated. Two of the main difficulties are, on the one hand, flow meters can disturb the flow patterns and, therefore, modify the measurements [51] and, on the other hand, the measurement methods must record the flow variations or, at least, the mean flow rate during a given period, for example, of 0.5 h [52]. Therefore, an alternative is to use indirect methods. The tracer gas decay technique is commonly used to characterize the natural ventilation in single-zone buildings [53]. It has the advantage of not disturbing the flow patterns and is based on the following hypotheses: the tracer gas is homogeneously distributed indoors and the flow barely varies during the sampling period. During an experiment, the time required to reduce the tracer gas concentration by 64 % (characteristic time, τ) can be obtained by fitting the time evolution of its concentration to an exponential decay of type:

$$I_C(t) = I_\infty + I_0 e^{-\frac{t-t_0}{\tau}} \quad (\text{Eq. 5})$$

where I_∞ and I_0 are the concentrations at t_∞ and t_0 respectively.

Here, we assume that the infiltrated NO_x into the room (through the non-hermetic elements of the building envelope) behaves as a tracer gas, before opening the window its concentration is homogeneously distributed indoors and after opening the window its concentration varies more rapidly than the flow. Therefore, using an individual passive scalar transport equation for dispersion of infiltrated NO_x , $I_C(t)$, allows quantifying τ by fitting the time evolution of its concentration to Eq. 5. The established indoor NO_x

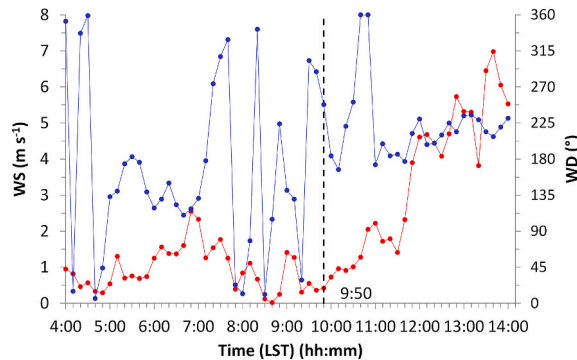


Fig. 3. WS and WD time evolution at TOWER (54.29 m AGL).

concentration when room ventilation starts (at 8:40 LST), I_0 , is $115 \mu\text{g m}^{-3}$. Note that infiltration time evolution before opening the window is not simulated in this work.

Finally, to check the tracer gas decay technique consistency, the ACHs are used. The ACH index is commonly used to characterize natural ventilation and it is equivalent to the number of air renewals per hour of a certain indoor volume of air. Here, the average ACH, $\langle ACH(t) \rangle$, is computed since the window is opened up to the infiltrated NO_x concentration is reduced by 95 % from CFD simulation using Eq. 6,

$$\langle ACH(t) \rangle = \frac{\langle \dot{m}(t) \rangle}{\rho V} \quad (\text{Eq. 6})$$

where $\langle \dot{m}(t) \rangle$ the CFD time evolution mass flow rate through the window, ρ is the air density (1.24 kg m^{-3}) and V is the room volume (112.5 m^3).

3. Results and discussion

3.1. Mesh sensitivity test

It is very important to define the correct mesh resolution indoors, outdoors close to the room, and on the outdoor-indoor interface (at the location of the opened window) to correctly simulate all the processes implied in the indoor-outdoor pollutant exchange. To ensure the independence of the model results with meshing, a mesh test is carried out. First, variations of ΔS_{\min} , from 0.25 m^2 to 2 m^2 are tested (Table 2) and then, the sensitivity to the number of sublayers into PLs at both sides of the outdoor-indoor interface (from 1 to 4) is examined.

Four meshes are built varying ΔS_{\min} but with only 1 sublayer into PLs: Mesh_1 (the finest), Mesh_2, Mesh_3 and Mesh_4 (the coarser). The typical ΔS_{\min} sizes and the total number of cells (N° Cells) of each one, are summarized in Table 2. The differences in number of cells are substantial due to the implied refinements around the surfaces.

Steady simulations for west WD and logarithmic vertical profiles for WS (and the typical forms of k and $\varepsilon(z)$ for a neutral profile, Eqs. 2–4) are carried out considering 3.6 m s^{-1} at 10 m height. Vertical profiles of normalized NO_x concentration, C_{norm} , are compared at different locations: indoor (IN), outdoor close to the room (OUT_n) and next to the emissions (OUT_f). C_{norm} (dimensionless) is defined as:

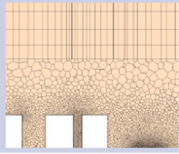
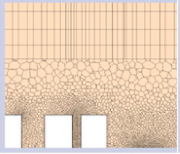
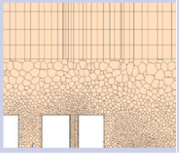
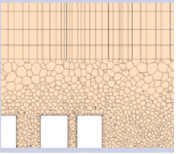




$$C_{norm} = \frac{C u^*}{E_C} \quad (\text{Eq. 7})$$

where C_{norm} is the CFD concentration and E_C is the total NO_x emission.

The results for each mesh are shown in Fig. 4. All vertical profiles are very similar at OUT_f , except close to the ground where the results of Mesh_4 differ from those of finer meshes. Moreover, at OUT_n and IN, not only the results of Mesh_4 differ from those of finer meshes, but also the results of Mesh_3.

However, the results of Mesh_2 and Mesh_1 are very similar both outdoors and indoors, but especially outdoors. Therefore, it can be concluded that Mesh_2 represents a good compromise between accuracy and number of cells.

Table 2
Meshing characteristics. Frontal and horizontal mesh views around the traffic emissions and buildings (up), indoors, and around the room (down) respectively.

Mesh_	1	2	3	4
ΔS_{\min} (m)	0.25	0.5	1	2
N° Cells (Indoor)	23.6×10^6 (3245)	11.2×10^6 (1643)	5.3×10^6 (507)	2.6×10^6 (177)
VERTICAL				
HORIZONTAL				

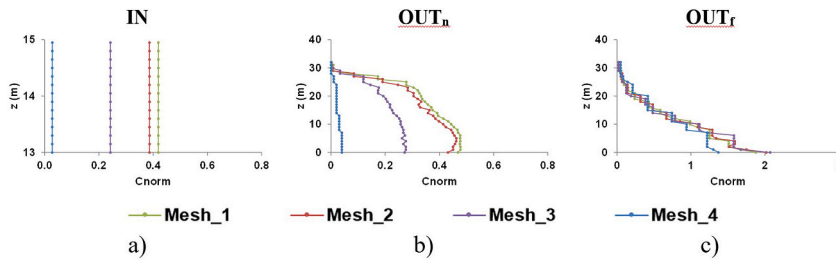
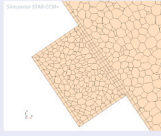
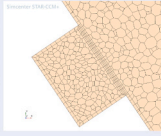
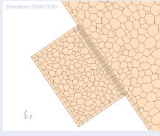
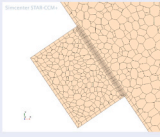


Fig. 4. Vertical profiles of C_{norm} at: a) IN, b) OUT_n and c) OUT_r .

Table 3
Meshing characteristics. Frontal mesh views in and around the room.

Mesh_2_	1 PL	2 PL	3 PL	4 PL
N° Cells (Indoor)	11.2×10^6 (1643)	11.2×10^6 (1792)	11.2×10^6 (1941)	11.2×10^6 (2136)
HORIZONTAL				

Secondly, four different meshes are built from Mesh_2 varying the number of sublayers into PLs from 1 to 4: Mesh_2_1P, Mesh_2_2 PL, Mesh_2_3 PL and Mesh_2_4 PL. The number of cells of each one are summarized in Table 3. As can be appreciated, the differences in number of cells are negligible.

In Fig. 5, the results for each mesh at OUT_n and IN are shown. At the outdoor site (OUT_n) all profiles are equal in all cases but indoor (IN), there are certain differences between meshes with 1 or 2 sublayers into PLs and meshes with 3 or 4 sublayers into PLs. Since the indoor results of Mesh_2_3 PL and Mesh_2_4 PL are very similar, Mesh_2_3 PL is chosen because the number of cells is lower.

Highlight how these results evidence the importance of the mesh resolution at indoor, outdoor close to the classroom and just into the outdoor-indoor interface (at the opening) to correctly capture the pollutants exchange by natural ventilation.

Finally, mesh quality of Mesh_2_3 PL has been verified checking that the limit values of the cell and boundary skewness angle, face validity, cell quality and volume change are within the established ranges [54].

Therefore, it can be concluded that the model results are independent of the mesh and the mesh quality is adequate.

3.2. Meteorology

The model is evaluated from the urban meteorology point of view to determine its capacity to correctly simulate the airflows above the buildings and around the San Carlos Hospital, i.e., inside the surrounding streets. This evaluation is essential to be confident in the pollutant dispersion simulations. For that, measurements of WS and WD at street level, GROUND point, and above the buildings, ROOF point, are used. In addition, measurements of κ at ROOF point are also employed.

The experimental and numerical WS and WD time evolutions are shown in Fig. 6. In addition, the observed time evolution of T_u and T_d from meteorological tower are also depicted.

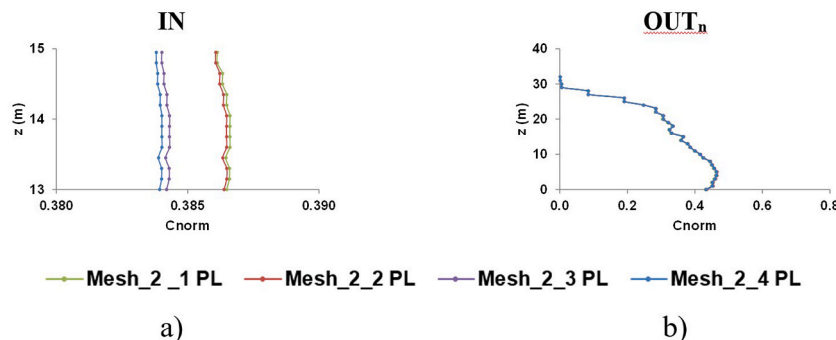


Fig. 5. Vertical profiles of C_{norm} at: a) OUT_n and b) IN.

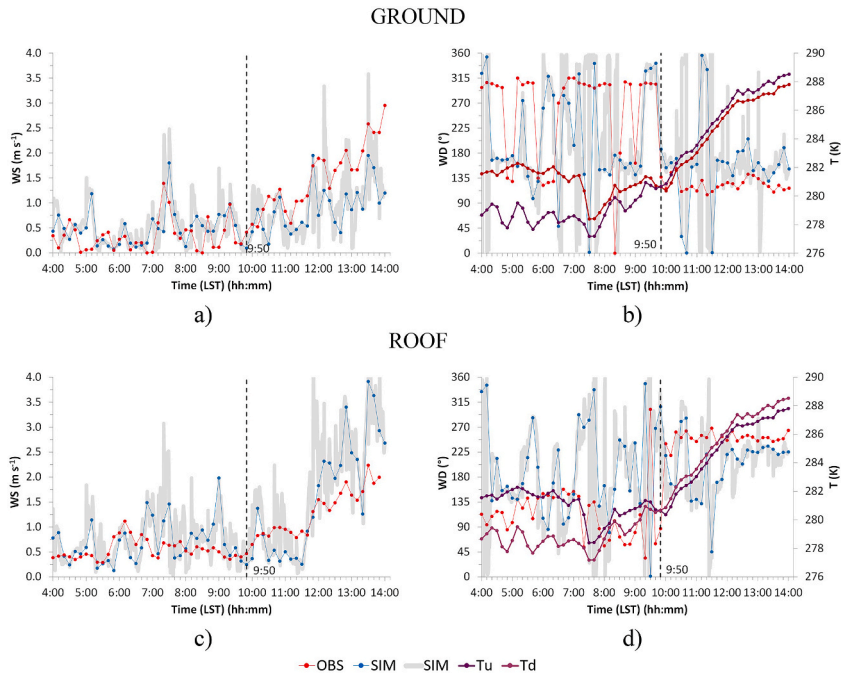


Fig. 6. Observed (red points, 10 min time series) and simulated (blue points, 10 min time series, and grey points, 1 s time series) of: a) WS at GROUND point; b) WD at GROUND point; c) WS at ROOF point; d) WD at ROOF point. In addition, experimental 10 min time series of T at TOWER (at 54.29 m and 3.6 m AGL) are shown (b and d).

Two well-marked regimes were observed during the test: the first one, from 4 LST up to 9:50 LST, which is characterized by relatively low WS (typically $< 1 \text{ m s}^{-1}$) and strong WD fluctuations and, the second one, from 9:50 LST up to 14 LST, which is characterized by a progressive increase in WS (typically $> 1 \text{ m s}^{-1}$) and practically constant WD (SE at GROUND, and SW at ROOF), mainly due to the channelling of the airflows within the streets. The regime changes at 9:50 LST is due to the change in atmospheric thermal stability, as shown T measured at TOWER, and it is related to thermally-driven flows present at this zone for weak synoptic condition [55].

To evaluate the model performance, the statistical parameters: correlation coefficient, R, normalized mean square error, NMSE, fractional bias, FB, and factor 2, FAC2 [56], are computed (Table 4) through the comparison between observed and simulated values.

For WS, the statistical parameters are acceptable at both locations (all of them verify $R > 0.633$; $\text{NMSE} < 0.493$; $\text{FB} < -0.052$; $\text{FAC2} > 0.750$), although they are better at ROOF, which was expected, as airflow is more perturbed near the surface. In general, at both locations, the model slightly overestimates WS ($\text{FB} < 0$) and, in particular, at ROOF, the relative error, RE, of WD is 75 % at 9 LST, 44 % at 12:50 LST and 43 % at 13:30 LST. For WD, the model does not seem to capture adequately the regime change occurring at 9:50 LST but it reproduces it somewhat later. However, during most of the simulated period, it reasonably reproduces both, trends and values.

Two regimes are also observed for turbulence conditions, evaluated from κ (Fig. 7): one with lower turbulence (up to 9:50 LST), and another (from 9:50 LST) where κ increases. It is observed that the numerical model captures appropriately the time evolution (a high R) but underestimates the values (high NMSE and FB and a low FAC2). Previous studies have shown how the Realizable $k - \epsilon$ turbulence model often underestimates κ [57]. Besides, the atmospheric thermal effects (which can increase the turbulence) are neglected in this simulation, although the thermal convection in winter (the day simulated) is much weaker than in summer.

3.3. Outdoor-indoor NO_x concentrations

Since the urban background NO_x concentration is a fundamental input for this type of simulations [58], first, the impact of using

Table 4
Statistical parameters comparing experimental and numerical results at GROUND and ROOF points.

	GROUND		ROOF	
	WS		WS	κ
R	0.633		0.816	0.855
NMSE	0.493		0.279	1.155
FB	-0.052		-0.029	1.471
FAC2	0.750		0.883	0.150

ROOF

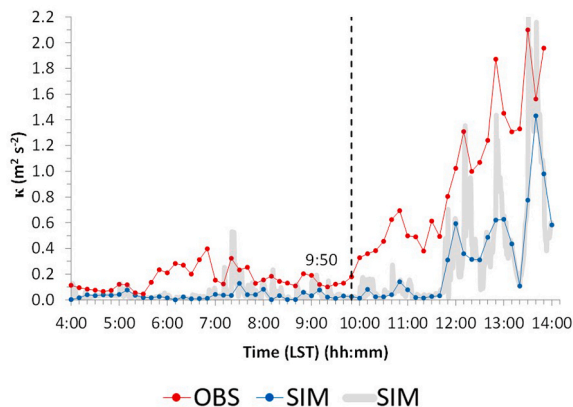


Fig. 7. Experimental (red points, 10 min time series) and numerical (blue points, 10 min time series, and grey points, 1 s time series) time evolution of κ above the buildings, ROOF location.

different $UB_{C_i}(t)$, on NO_x concentrations, particularly outdoors, is evaluated. Four urban background AQMS located at different distances and in different directions from the study area are selected. These locations are named as their local sites: Retiro (at approx. 4 km to the SE), Farolillo (at approx. 5 km to the SO), Tres Olivos (at approx. 7 km to the NE) and Arturo Soria (at approx. 8 km to E) (see supplementary material, Figure SM4). These urban backgrounds are simulated considering two cases: 1) neglecting any delay due to the time taken for transport polluted air masses from the urban background AQMS locations to the studied domain boundaries, and 2) taking into account the possible delay by transport of air masses. This delay was estimated analysing the lag with higher cross-correlation between experimental NO_x concentrations at GROUND and OUT locations, and the chosen $UB_{C_i}(t)$.

The experimental and numerical time evolutions of NO_x concentrations are shown in Fig. 8 and Fig. 9 at GROUND and OUT locations, with the following characteristics:

- without time lags (SIM)
- with time lags (SIM_Lag)
- with time lags + ambuances (SIM_Lag + A_k)

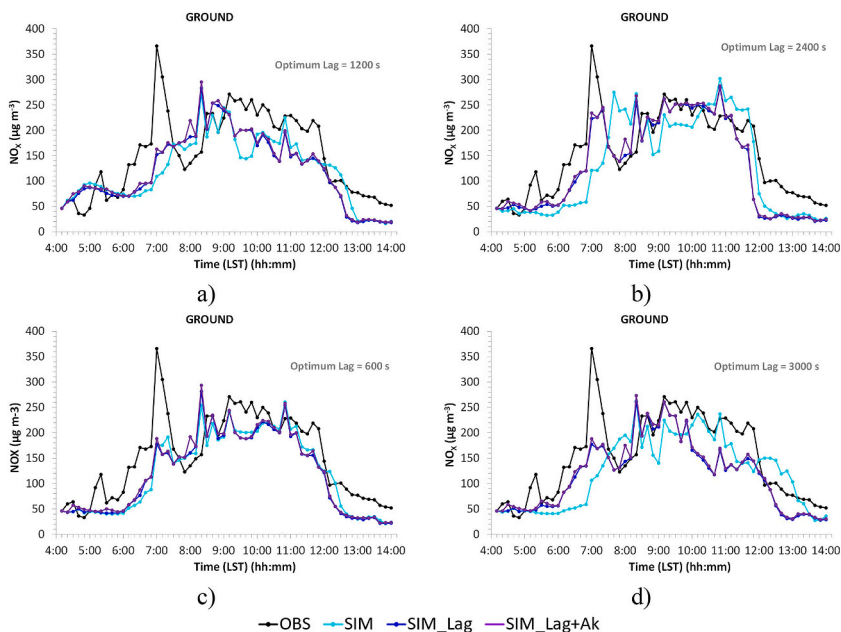


Fig. 8. Experimental (black points) and numerical time evolution of NO_x concentrations: without time lags (light blue points), with time lags (dark blue points) and with time lags + ambuances (purple points) at GROUND location, and with urban background concentrations from AQMS: a) Retiro, b) Farolillo, c) Tres Olivos and d) Arturo Soria.

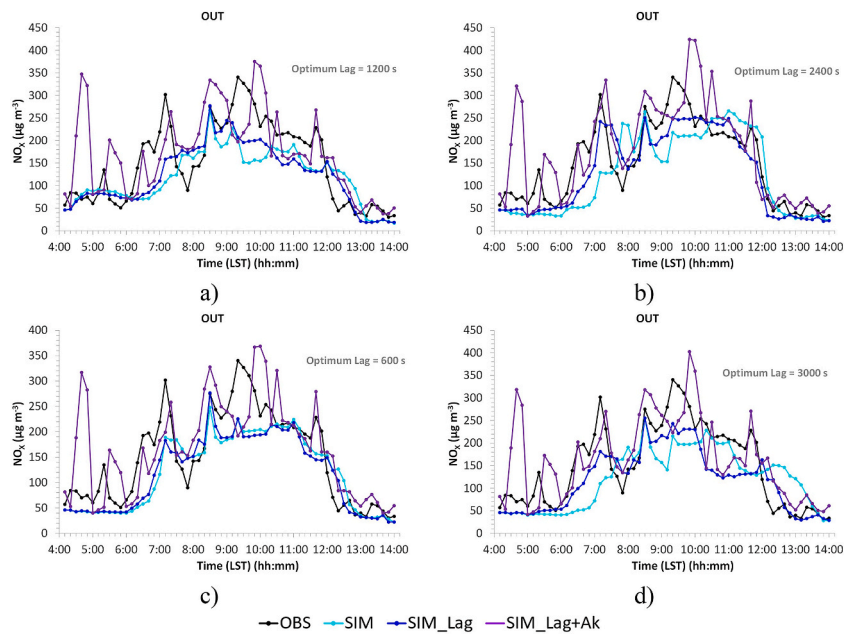


Fig. 9. Experimental (black points) and numerical time evolution of NO_x concentrations without time lags (light blue points), with time lags (dark blue points) and with time lags + ambulances (purple points) at OUT location, and urban background concentrations from AQMS: a) Retiro, b) Farolillo, c) Tres Olivos and d) Arturo Soria.

Outdoor NO_x observational concentrations are high (typically > 200 µg m⁻³), especially between 7 LST and 12 LST. This behaviour (high NO_x concentrations from early morning up to midday during the weekdays of wintertime) is due to the combination of high traffic emissions and very stable meteorological conditions including low-level thermal inversion layer, which is unfavourable for pollutant dispersion [33,19].

Besides, two peaks are appreciated within this period, the first one around 7 LST and the second one around 9:30 LST. The peak of 7 LST is observed both at OUT (302 µg m⁻³) and GROUND (366 µg m⁻³) locations and is typical in cities like Madrid [59]. However, the peak of 9:30 LST is only observed at OUT location (340 µg m⁻³).

Regarding the numerical results without time lags and with time lags, the four simulated $UB_{C_i}(t)$ fit the experimental results quite well, both in trends and in values, especially when the time lags are taken into account. Particularly, the NO_x peak at 7 LST is better simulated when 2400 s-lagged urban background concentration data from the Farolillo station are used, but not reaching the magnitude of the peak.

However, the peak of 9.30 LST does not seem affected by the urban background since the numerical results are not improved with the time lags. Hence, it is reasonable to think that it could be due to other local emissions, closer to the OUT location than GROUND location, such as parked ambulances around the hospital with the engine idling. This hypothesis is compatible with numerical results with time lags and ambulances since their contribution at OUT location gives rise to a peak of an adequate size but slightly delayed from the real (around 30 min). This delay could be related to the fact that the model, as mentioned above, does not seem to capture the WD change at the right time and/or the WS peak between 8:50 LST and 9:10 LST inhibits the increase of concentration that occurs between 9 and 9:20 LST at OUT location (see § 3.2). Note that the ambulances' contribution to the peak of 7 LST at OUT location could be also important, as numerical results with time lags and ambulances have shown. In addition, it is important to note that the contribution from ambulances is modelled as time-constant emissions assuming they are parked with the engine idling throughout the entire day, although in reality the movement of ambulances around the hospital is more complex. These results show that emission sources in the immediate vicinity of the room can contribute significantly to the total concentration despite their emissions are lower compared to other pollutant sources further away (see § 2.1).

Table 5
Statistical parameters comparing experimental and numerical results at GROUND location.

	Retiro			Farolillo			Tres Olivos			Arturo Soria		
	SIM	SIM_Lag	SIM_Lag + Ak	SIM	SIM_Lag	SIM_Lag + Ak	SIM	SIM_Lag	SIM_Lag + Ak	SIM	SIM_Lag	SIM_Lag + Ak
R	0.685	0.766	0.756	0.727	0.882	0.877	0.859	0.851	0.844	0.688	0.854	0.847
NMSE	0.200	0.159	0.153	0.197	0.093	0.090	0.115	0.126	0.119	0.197	0.137	0.128
FB	0.257	0.291	0.258	0.365	0.348	0.310	0.325	0.347	0.310	0.255	0.307	0.274
FAC2	0.800	0.817	0.833	0.650	0.717	0.717	0.750	0.750	0.783	0.817	0.917	0.933

Table 6
Statistical parameters comparing experimental and numerical results at OUT location.

	Retiro			Farolillo			Tres Olivos			Arturo Soria		
	SIM	SIM_Lag	SIM_Lag + Ak	SIM	SIM_Lag	SIM_Lag + Ak	SIM	SIM_Lag	SIM_Lag + Ak	SIM	SIM_Lag	SIM_Lag + Ak
R	0.708	0.812	0.621	0.743	0.900	0.770	0.839	0.863	0.702	0.658	0.878	0.696
NMSE	0.227	0.151	0.214	0.192	0.078	0.159	0.138	0.131	0.167	0.246	0.132	0.164
FB	0.177	0.198	-0.176	0.297	0.264	-0.155	0.249	0.267	-0.144	0.192	0.227	-0.163
FAC2	0.850	0.933	0.833	0.833	0.833	0.900	0.900	0.933	0.867	0.833	0.983	0.850

To evaluate the outdoor model performance, the previous statistical parameters: R, NMSE, FB and FAC2, are computed at OUT and GROUND locations (Table 5 and Table 6). Statistical parameters without time lags are quite good (all of them verify $R > 0.658$; $NMSE < 0.246$; $FB < 0.365$; $FAC2 > 0.650$) but they improve with time lags (all of them verify $R > 0.766$; $NMSE < 0.159$; $FB < 0.348$; $FAC2 > 0.717$).

Note that, at GROUND location, the ambulances are far enough away that their impact is negligible. However, at OUT location, the model simulations with time lags but without ambulances underestimate outdoor NO_x concentrations ($FB > 0$), but with time lags and ambulances it is the opposite ($FB < 0$). This is because it has been assumed that the ambulances were constantly parked around the hospital with the engine idling due to non-available information about ambulance counts and paths around the hospital during the test. The results show that their contribution to the total concentration can be important although their emissions may be lower compared to other pollutant sources further away.

It is concluded that data from all studied background AQMS can be used as background NO_x contribution in the CFD simulations considering an appropriate time lag. Given these results, simulation using the lagged NO_x concentration recorded in the Retiro AQMS is chosen to evaluate if the model is capable of properly reproducing the outdoor-indoor NO_x exchange, and to analyse the impact of each contribution (urban background, traffic emissions in streets surrounding the Hospital and local emissions such as parked ambulances around the hospital with the engine idling) on indoor NO_x concentration.

In Fig. 10 a, the experimental and modelling time evolutions of NO_x concentrations:

- without time lags (SIM)
- with time lags (SIM_Lag)
- with time lags + ambulances (SIM_Lag + A_k)

at IN location when the room was being naturally ventilated through an open window are shown. In addition, the time evolutions of experimental and modelled (for SIM_Lag) I/O is also depicted. Note that I/O concentration ratios are computed using NO_x concentration at IN and OUT locations. Fig. 10 b shows the time evolutions of the contributions, in %, from each NO_x source to the total indoor NO_x concentration for SIM_Lag A_k case.

Note that, time evolution of infiltrated NO_x concentration into the room through building envelope before opening the window is not simulated here. Indoor NO_x concentration at time of window opening is imposed in the simulations as an initial indoor NO_x concentration. The time evolution of this contribution is shown in Fig. 10 b as “Infiltrated NO_x ”.

As observed in the experimental results, NO_x concentration at IN location, reaches high values (typically $> 200 \mu g m^{-3}$), especially between 8:40 LST and 12 LST and the peak of 9:30 LST is well appreciated ($274 \mu g m^{-3}$). Between 8:40 LST and 12 LST indoor NO_x concentration is similar to outdoor concentration (experimental I/O is around 0.8 and modelled I/O close to 1). This is because between 8:40 LST and 12 LST, natural ventilation of room is efficient enough so that the indoor NO_x concentration time evolution can follow outdoor NO_x concentration time evolution, although slightly damped. Between 12 LST and 13 LST, NO_x concentration at OUT location rapidly decreases due to the rapid increase of WS and turbulence (including thermal convection) above the canopy (see Fig. 6

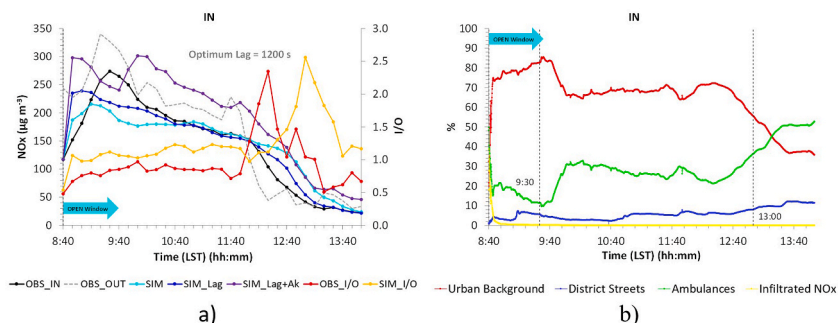


Fig. 10. a) Experimental (black points) and numerical time evolution of NO_x concentrations without time lags (light blue points), with time lags (dark blue points) and with time lags and ambulances (purple points) and experimental (red points) and numerical time evolution of I/O (orange points) at IN location, Background concentration taken from Retiro AQMS; b) contributions, in %, from urban background (in red), district streets (in blue), ambulances (in green) and infiltrated NO_x (in yellow) on total indoor NO_x concentration.

c), causing the ventilation of streets. However, for this period, I/O increases above 1 (i.e., indoor concentration is higher than outdoor) due to the natural ventilation of the room is not efficient enough to follow the rapid variation of outdoor concentration (indoor turbulence is lower than outdoor turbulence). The indoor-outdoor exchange is limited by room ventilation, preventing the rapid decrease in indoor NO_x concentration. However, from 12 p.m., I/O is variable (experimental I/O ranges from 2.4 to 0.5 respectively and modelled I/O from 2.5 to 1). These results show how, in real situations, variations of I/O can be strong and depends not only the current conditions but also the previous one.

As showed in Fig. 10 a, where the NO_x concentrations without time lags and with time lags are shown, numerical results fit experimental measurements appropriately, in both values and trend, especially when time lags are taking into account, except during the peak of 9:30 LST. As expected, the failure of the model to predict the outdoor NO_x concentrations during the peak of 9:30 LST is transferred to the indoor. About indoor-outdoor NO_x concentration ratio, between 8:40 LST and 12 LST, numerical results fit experimental values and trend reasonably well (average value 1.1). However, from 12 LST, numerical results seem to reproduce experimental results with some delay. This is probably because the transient period between 12 LST and 13 LST is captured with some delay.

To evaluate the indoor performance of the model, the same statistical parameters were computed (Table 7). As expected, statistical parameters without time lags are very good (all of them verify $R > 0.917$; $NMSE < 0.048$; $FB > 0.105$; $FAC2 = 0.550$), and, in general, they improve with time lags (all of them verify $R > 0.939$; $NMSE < 0.028$; $FB > 0.039$; $FAC2 = 0.550$).

As mentioned above, the parked ambulances around the hospital with engine idling could be an important contribution to outdoor NO_x concentrations at the OUT location. Hence, it has been also analysed their impact on indoor NO_x concentrations at the IN location. Their contribution (mainly of those parked on the corner of the Hospital's east wing, just below the room) to the total indoor NO_x concentration could be between 10 % and 50 %, depending on the environmental conditions (Fig. 10 b).

Moreover, although in general, the major contribution to the total indoor NO_x concentration comes from the urban background (ranges from 38 % to 86 %, Fig. 10 b), it is observed that, under certain environmental conditions, the local emissions (for example, at 14 LST) become dominant. However, district streets contribution is always the minor contribution to indoor NO_x concentration (between 2 % and 12 %, Fig. 10 b) due to the window of the room is located more than 80 m away from the nearest street.

The impact of environmental conditions on percentage contributions from urban background, ambulances and district streets was investigated in a previous theoretical study focusing on the same room [60]. It was observed that WD is the most influential factor, particularly when the room is at the leeward façade (see supplementary material, Figure SM5)

Therefore, to understand the behaviour of percentage contributions, two times are analysed hereinafter: 1) 9:30 LST and 2) 13 LST with opposite WD (considering the room at the windward and leeward respectively). At 9:30 LST, the urban background contribution was increasing and the ambulances contribution was decreasing and at 13:00 LST, the contrary is observed.

The tangential component of the velocity field and high-resolution maps of total NO_x concentration and NO_x concentration due to ambulances in a vertical plane section passing through the centre of the room at these two times are shown in Fig. 11.

At 9:30 LST, the room is at the windward facade of the hospital and the outdoor configuration is characterized by the formation of a vortex in front of the room that rotates counter clockwise. This vortex, on the one hand, favours the pollutants coming from the urban background enter to the room from above (Fig. 11 a), increasing the contribution of this source to indoor NO_x concentration. And, on the other hand, it prevents the pollutants coming from the parked ambulances just below the room enter to the room from below (Fig. 11 b), reducing the contribution of this source to the indoor NO_x concentration.

Instead, at 13 LST, the room is at the leeward facade of the hospital and the outdoor configuration is characterized by the formation of a vortex in front of the room, slightly shifted up from the previous one, which rotates clockwise. In this case, the vortex prevents the pollutants coming from the urban background enter to the room (Fig. 11 c), reducing the contribution of this source to indoor NO_x concentration, and, favouring the pollutants coming from the ambulances enter to the room (Fig. 11 d), increasing the contribution of this source to the indoor NO_x concentration.

Note that, both times belong to peak hours (Figure SM3) but 9:30 LST time is included in the lower WS regime (inlet WS is 0.55 m s^{-1} , Fig. 3, and $UB_{C_{Retiro}} = 192 \mu\text{g m}^{-3}$) and 13 LST time is included in the higher WS regime (inlet WS is 5.32 m s^{-1} , Fig. 3, and $UB_{C_{Retiro}} = 14 \mu\text{g m}^{-3}$).

These results highlight the importance of the environmental conditions in outdoor-indoor NO_x exchange by natural ventilation, particularly the WD.

The impact of the heating on the outdoor-indoor NO_x exchange is also investigated. The experimental and numerical time evolutions of NO_x concentrations are shown in Fig. 12:

- with time lags (SIM_Lag)
- with time lags + HS (SIM_Lag + HC)

at OUT and IN locations respectively.

Numerical results show how, when the window is opened (from 8:40 LST to 14 LST), outdoor NO_x concentration hardly changes with the HS presence, but indoor NO_x concentration decreases slightly (average relative difference of 9 %). As expected, the exchange outdoor-indoor concentration is more effective due to stack pressure contribution but the differences with and without HS on I/O are low.

Finally, SSV of the room is analysed using the infiltrated NO_x concentration decay and the ACHs. The numerical time evolution and exponential fit of infiltrated NO_x concentration at IN location when the room was being single-sided naturally ventilated through an open window are shown in Fig. 13.

Table 7
Statistical parameters comparing experimental and numerical results at IN location.

	Retiro		
	SIM	SIM_Lag	SIM_Ak_Lag
R	0.917	0.939	0.918
NMSE	0.048	0.028	0.112
FB	-0.105	-0.039	-0.401
FAC2	0.550	0.550	0.550

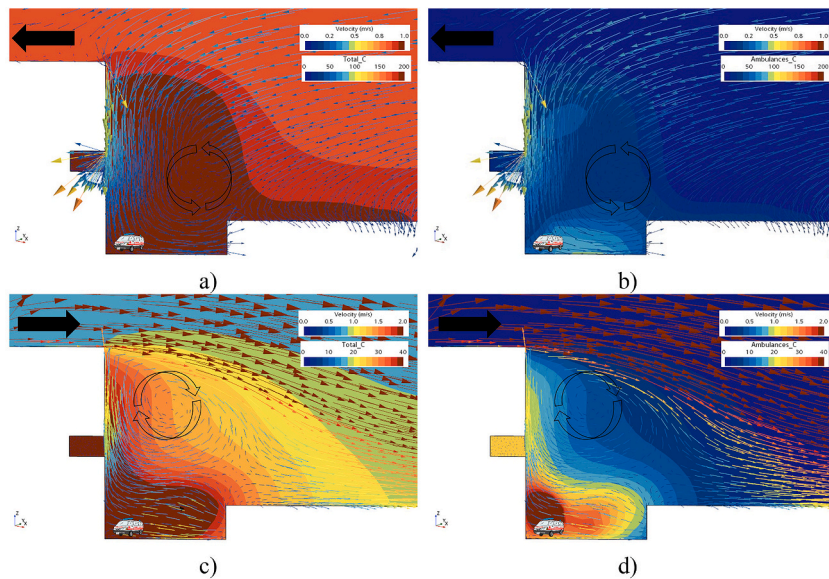


Fig. 11. Zoom of the tangential component of the velocity field and high-resolution maps of: a) total NO_x concentration at 9:30 LST, b) NO_x concentration due to ambulances at 9:30 LST, c) total NO_x concentration at 13 LST and d) NO_x concentration due to ambulances at 13 LST, in a vertical plane section passing through the centre of the room. Large black arrows indicate prevailing WD at roof level.

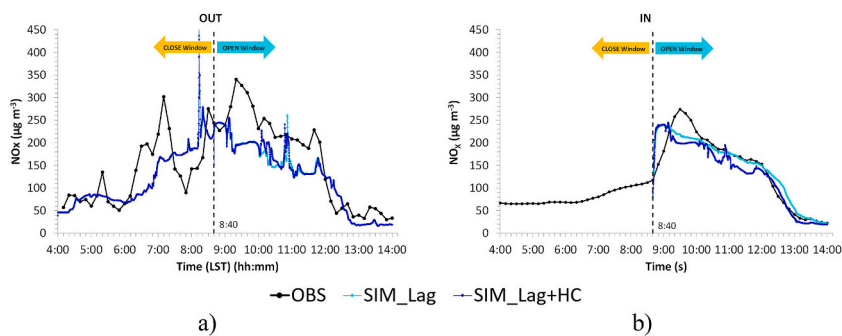


Fig. 12. Experimental (black points) and numerical time evolution of NO_x concentrations, with time lags (light blue points) and with time lags and HS (dark blue points) at a) OUT location and b) IN location. Background concentration taken from Retiro AQMS.

As can be seen, numerical results fit well to Eq. 5 (R^2 is 0.974) and for this case, the obtained τ is 67.725 s. So, 3τ , which is time required to reduce the indoor pollutant concentration by 95 %, is approximately 3.4 min (equivalent to $ACH = 17.65 \text{ h}^{-1}$). In addition, $\langle ACH(t) \rangle$, has been computed from CFD simulation using Eq. 6 and both results have been compared. The obtained CFD value is 15.56 h^{-1} , which is consistent with 3τ . Therefore, in this case, the infiltrated NO_x concentration decay technique is effective.

This exercise illustrates how the CFD methodology yields similar results to simple empirical models. However, CFD methodology, in addition, allows varying both meteorological conditions and geometric parameters to look for relationships between both and SSV of the room, which would be very useful for improvement the simple models.

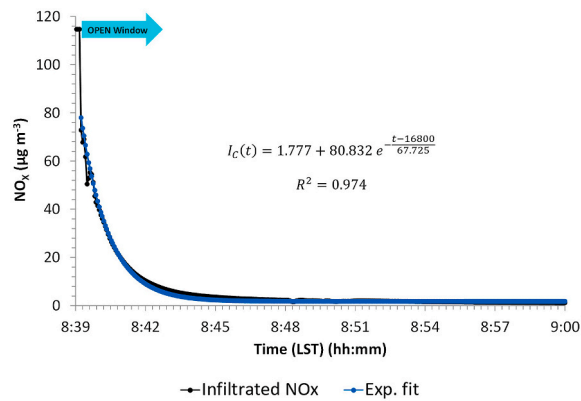


Fig. 13. Numerical time evolution (black points) and exponential fit (blue points) of infiltrated NO_x concentration at IN location.

4. Conclusions

The traffic-related indoor-outdoor air pollution in a real single-sided naturally ventilated room is addressed applying a CFD model. The model simulates explicitly the outdoor-indoor NO_x exchange time-evolution in a room located on the 4th floor of *San Carlos* Hospital east wing on February 18, 2021, from 4 LST to 14 LST.

The sensitivity tests performed highlight the importance of the mesh resolution indoors, and outdoors in the immediate vicinity of the building to capture the pollutants exchanged by natural ventilation. Our results also point out that the combination of the URANS turbulence approach with suitable boundary conditions appropriately reproduces the time evolution of meteorological variables (WD, WS and k), both inside the streets and above the buildings, even for low WS (typically $< 1 \text{ m s}^{-1}$). A Large Eddy Simulation (LES) turbulence model would be more accurate but more expensive from the computational point of view. However, on one hand, experimental data are averaged every 10 min and, on the other hand, URANS simulation provided suitable results. Hence, considering the size of this geometrical domain and the computational time required, this approach is a good compromise between accuracy and computational cost. The time evolution of outdoor and indoor NO_x concentrations is appropriately simulated too, in particular, when the urban background is properly modelled from AQMS data. The results from this case study suggest that it is more important to account for the delay of arriving air masses from the urban background AQMS to the domain boundary than the urban background AQMS chosen for this type of unsteady simulations. In these cases, NO_x urban background concentrations significantly contribute to the indoor NO_x concentration. Nonetheless, the contribution from local sources seem to be relevant to explain some details of observed NO_x concentration time series. In this particular study, the results show that idling ambulances just below the room can contribute between 10 % and 50 % to the total indoor NO_x concentration, even when their emissions are considerably smaller than those of traffic in nearby streets. This is because indoor NO_x concentration (in the absence of indoor pollutant sources) is intrinsically related to the wind flow around the hospital facade where the window is located. Therefore, depending on the outdoor WD (studied facade at windward or leeward), the local emissions compete with urban background for the major contribution to the indoor NO_x concentration. Taking into account this fact, natural ventilation should be done during hours of low air pollutant concentrations, avoiding peak hours in the morning and the evening. Additionally, one way to promote natural ventilation in urban environments would be to reduce pollutant concentrations close to the windows, for example, implementing measures for reducing traffic around buildings, especially in areas with sensitive populations, such as hospitals, schools, nursing homes, etc. In cases where these types of measures cannot be implemented, it would be interesting to promote the use of systems that allow the natural ventilation of buildings can be smartly managed (i.e. during the hours in which the outdoor air quality is more favourable) and to promote the use of less polluting engines. I/O is not constant over time during the test. Just when the window is opened, the concentration just outside of the window is higher than the indoor concentration (by almost 50 %) and, due to the strong initial indoor-outdoor concentration and pressure gradients, it quickly disperses into the room, being I/O close to 1 in few minutes. This ratio keeps practically constant during 3 h approximately. Later, the environment ventilation improves due to the turbulence increasing; however, I/O is greater than 1. This is because indoor concentration slowly decreases due to the limited ventilation of the room (in this case, type SSV, which does not favour the room ventilation). These results show how I/O depends not only on the outdoor concentration (which, at the same time, depends on the atmospheric turbulence), but also on the kind of ventilation, showing a wide range of values. In addition, we should keep in mind that the OUT location is outdoor, but just located close to the window and other outdoor locations at pedestrian levels in the sidewalks provide different I/O values due to the strong gradient of concentration at the street level [60], which is an important issue to be addressed in future studies. The simulation done using a HS in the room illustrate how an internal thermal load modifies the natural ventilation and, therefore, impacts indoor pollutant concentrations. Here, the impact of 1500 W heater below the open window is low. Notwithstanding, a more detailed study would be needed about possible heat sources in the room because under certain meteorological conditions the stack pressure effect could be more important than the wind pressure effect.

The time required to ventilate the room is 3.4 min. It has been obtained using the infiltrated NO_x concentration decay and has been verified through the $\langle ACH(t) \rangle$. This result shows the potential of time-dependent CFD simulations for characterizing the natural ventilation of single-zone buildings. In addition, CFD methodology would be very useful for designing parameterizations of natural

ventilation for simpler models, because they let relate τ and the meteorological conditions depending on the type of neighbourhood/building/room/window.

CRedit authorship contribution statement

E. Rivas: Conceptualization, Data curation, Formal analysis, Investigation, Methodology, Supervision. **J.L. Santiago:** Conceptualization, Formal analysis, Investigation, Methodology, Supervision. **F. Martín:** Conceptualization, Formal analysis, Investigation, Methodology, Supervision. **A. Martilli:** Conceptualization, Formal analysis, Investigation, Methodology, Supervision. **E. Díaz:** Data curation, Formal analysis, Investigation, Methodology, Supervision. **F.J. Gómez-Moreno:** Data curation, Formal analysis, Investigation, Methodology, Supervision. **B. Artiñano:** Data curation, Formal analysis, Investigation, Methodology, Supervision. **C. Román-Cascón:** Data curation, Formal analysis, Investigation, Methodology, Supervision. **C. Yagüe:** Data curation, Formal analysis, Investigation, Methodology, Supervision. **D. de la Paz:** Data curation, Formal analysis, Investigation, Methodology, Supervision. **R. Borge:** Data curation, Formal analysis, Investigation, Methodology, Supervision.

Declaration of competing interest

We wish to confirm that there are no known conflicts of interest associated with this publication and there has been no significant financial support for this work that could have influenced its outcome.

We confirm that the manuscript has been read and approved by all named authors and that there are no other persons who satisfied the criteria for authorship but are not listed. We further confirm that the order of authors listed in the manuscript has been approved by all of us.

We confirm that we have given due consideration to the protection of intellectual property associated with this work and that there are no impediments to publication, including the timing of publication, with respect to intellectual property. In so doing we confirm that we have followed the regulations of our institutions concerning intellectual property.

Data availability

Data will be made available on request.

Acknowledgements

This study has been supported by European Union-NextGenerationEU (UP2021-035) and by the AIRTEC-CM research project (S2018/EMT-4329) funded by The Regional Government of Madrid. The simulations were carried out in the Supercomputer *Turgalium* belonging to the Extremadura Research Centre for Advances Technologies (CETA-CIEMAT) from Spanish Government.

Appendix A. Supplementary data

Supplementary data to this article can be found online at <https://doi.org/10.1016/j.jobe.2023.108403>.

References

- [1] I. Manisalidis, E. Stavropoulou, A. Stavropoulos, E. Bezirtzoglou, Environmental and health impacts of air pollution: a review, *Front. Public Health*, 8, (2020) 14, <https://doi.org/10.3389/fpubh.2020.00014>.
- [2] World Health Organization, WHO global air quality guidelines: particulate matter (PM_{2.5} and PM₁₀), ozone, nitrogen dioxide, sulphur dioxide and carbon monoxide, 2021. Available at: <https://apps.who.int/iris/handle/10665/345329>.
- [3] H. Mayer, Air pollution in cities, *Atmos. Environ.* 33 (24–25) (1999) 4029–4037, [https://doi.org/10.1016/S1352-2310\(99\)00144-2](https://doi.org/10.1016/S1352-2310(99)00144-2).
- [4] R. Burnett, H. Chen, M. Szyszko, N. Fann, B. Hubbell, C.A. Pope III, J.V. Spadaro, Global estimates of mortality associated with long-term exposure to outdoor fine particulate matter, *Proc. Natl. Acad. Sci. USA* 115 (38) (2018) 9592–9597, <https://doi.org/10.1073/pnas.1803222115>.
- [5] R. Izquierdo, S.G. Dos Santos, R. Borge, D. de la Paz, D. Sarigiannis, A. Gotti, E. Boldo, Health impact assessment by the implementation of Madrid City air-quality plan in 2020, *Environ. Res.* 183 (2020) 109021, <https://doi.org/10.1016/j.envres.2019.109021>.
- [6] G. Hoek, R.M. Krishnan, R. Beelen, A. Peters, B. Ostro, B. Brunekreef, J.D. Kaufman, Long-term air pollution exposure and cardio-respiratory mortality: a review, *Environ. Health* 12 (1) (2013) 1–16, <https://doi.org/10.1186/1476-069X-12-43>.
- [7] L. Sheppard, J.C. Slaughter, J. Schildcrout, L.J. Liu, T. Lumley, Exposure and measurement contributions to estimates of acute air pollution effects, *J. Expo. Sci. Environ. Epidemiol.* 15 (4) (2005) 366–376, <https://doi.org/10.1038/sj.jea.7500413>.
- [8] J.L. Santiago, F. Martín, A. Martilli, A computational fluid dynamic modelling approach to assess the representativeness of urban monitoring stations, *Sci. Total Environ.* 454 (2013) 61–72, <https://doi.org/10.1016/j.scitotenv.2013.02.068>.
- [9] J.L. Santiago, F. Martín, Uso de modelos CFD para estimar la representatividad espacial de estaciones de medida de la contaminación atmosférica urbana y la idoneidad de sus ubicaciones, *Física de la Tierra* 27 (2015) 191–222, <https://doi.org/10.5209/rev.FITE.2015.v27.51200>.
- [10] O. Kracht, J. Santiago, F. Martín, A. Piersanti, G. Cremona, G. Righini, L. Vitali, K. Delaney, B. Basu, B. Ghosh, W. Spangl, C. Brendle, J. Latikka, A. Kousa, E. Pärjälä, M. Meretoja, L. Malherbe, L. Letinois, M. Beauchamp, F. Lenartz, V. Hutsemekers, L. Nguyen, R. Hoogerbrugge, K. Eneroth, S. Silvergren, H. Hooyberghs, P. Viaene, B. Maiheu, S. Janssen, D. Roet, M. Gerboles, Spatial representativeness of air quality monitoring sites: outcomes of the FAIRMODE/AQUILA intercomparison exercise, Publications Office, 2017. DOI: 10.2760/60611 Available at: <https://op.europa.eu/en/publication-detail/-/publication/ed931ea2-16ba-11e8-9253-01aa75ed71a1/language-en>.
- [11] C. Román-Cascón, C. Yagüe, R. Borge, P. Ortiz, E. Serrano, M. Sastre, G. Maqueda, B. Sánchez, B. Artiñano, F.J. Gómez-Moreno, E. Díaz-Ramiro, E. Alonso, J. Fernández, A. Martilli, J.M. Cordero, A. Narros, A.M. García, A. Núñez, Wind and turbulence relationship with NO₂ in an urban environment: a fine-scale observational analysis, *Urban Clim.* 51, (2023) 101663, <https://doi.org/10.1016/j.uclim.2023.101663>.

- [12] M.C. Nagl, M.I. Buxbaum, M.S. Böhmer, M.N. Ibesich, M.H.R. Mendoza, Air Quality and urban traffic in the EU: best practices and possible solutions, Available at: [https://www.europarl.europa.eu/RegData/etudes/STUD/2018/604988/IPOL_STU\(2018\)604988_EN.pdf](https://www.europarl.europa.eu/RegData/etudes/STUD/2018/604988/IPOL_STU(2018)604988_EN.pdf), 2018.
- [13] S. Vardoulakis, E. Solazzo, J. Lumbreras, Intra-urban and street scale variability of BTEX, NO₂ and O₃ in Birmingham, UK: Implications for exposure assessment, *Atmos. Environ.* 45 (29) (2011) 5069–5078, <https://doi.org/10.1016/j.atmosenv.2011.06.038>.
- [14] R. Borge, A. Narros, B. Artíñano, C. Yagüe, F.J. Gómez-Moreno, D. de la Paz, C. Román-Cascón, E. Díaz, G. Maqueda, M. Sastre, C. Quaassdorff, C. Dimitroulopoulou, S. Vardoulakis, Assessment of microscale spatio-temporal variation of air pollution at an urban hotspot in Madrid (Spain) through an extensive field campaign, *Atmos. Environ.* 140 (2016) 432–445, <https://doi.org/10.1016/j.atmosenv.2016.06.020>.
- [15] J.L. Santiago, R. Borge, F. Martín, D. De La Paz, A. Martilli, J. Lumbreras, B. Sanchez, Evaluation of a CFD-based approach to estimate pollutant distribution within a real urban canopy by means of passive samplers, *Sci. Total Environ.* 576 (2017) 46–58, <https://doi.org/10.1016/j.scitotenv.2016.09.234>.
- [16] Y. Peng, Z. Gao, R. Buccolieri, W. Ding, An investigation of the quantitative correlation between urban morphology parameters and outdoor ventilation efficiency indices, *Atmosphere* 10 (1) (2019) 33, <https://doi.org/10.3390/atmos10010033>.
- [17] World Health Organization, Combined or multiple exposure to health stressors in indoor built environments: an evidence-based review prepared for the WHO training workshop “Multiple environmental exposures and risks”, 16–18 October 2013, Bonn, Germany, 2014. Available at: <https://apps.who.int/iris/handle/10665/350495>.
- [18] E. Rivas, J.L. Santiago, Y. Lechón, F. Martín, A. Ariño, J.J. Pons, J.M. Santamaría, CFD modelling of air quality in Pamplona city (Spain): Assessment, stations spatial representativeness and health impacts valuation, *Sci. Total Environ.* 649 (2019) 1362–1380, <https://doi.org/10.1016/j.scitotenv.2018.08.315>.
- [19] B. Sánchez, J.L. Santiago, A. Martilli, F. Martín, R. Borge, C. Quaassdorff, D. de la Paz, Modelling NO_x concentrations through CFD-RANS in an urban hot-spot using high resolution traffic emissions and meteorology from a mesoscale model, *Atmos. Environ.* 163 (2017) 155–165, <https://doi.org/10.1016/j.atmosenv.2017.05.022>.
- [20] J.L. Santiago, R. Borge, B. Sanchez, C. Quaassdorff, D. De La Paz, A. Martilli, E. Rivas, F. Martín, Estimates of pedestrian exposure to atmospheric pollution using high-resolution modelling in a real traffic hot-spot, *Sci. Total Environ.* 755 (2021) 142475, <https://doi.org/10.1016/j.scitotenv.2020.142475>.
- [21] J.L. Santiago, E. Rivas, R. Buccolieri, A. Martilli, M.G. Vivanco, R. Borge, F. Martín, Indoor-outdoor pollutant concentration modelling: A comprehensive urban air quality and exposure assessment, *Air Qual. Air Quality, Atmos. & Health* 15 (9) (2022) 1583–1608, <https://doi.org/10.1007/s11869-022-01204-0>.
- [22] J. Sundell, H. Levin, W.W. Nazaroff, W.S. Cain, W.J. Fisk, D.T. Grimsrud, F. Gyntelberg, Y. Li, A.K. Persily, A.C. Pickering, J.M. Samet, J.D. Spengler, S.T. Taylor, C.J. Weschler, Ventilation rates and health: multidisciplinary review of the scientific literature, *Indoor air* 21 (3) (2011) 191–204, <https://doi.org/10.1111/j.1600-0668.2010.00703.x>.
- [23] T.M. Mata, A.A. Martins, C.S. Calheiros, F. Villanueva, N.P. Alonso-Cuevilla, M.F. Gabriel, G.V. Silva, Indoor Air Quality: A Review of Cleaning Technologies, *Environments* 9 (9) (2022) 118, <https://doi.org/10.3390/environments9090118>.
- [24] Z. Tong, Y. Chen, A. Malkawi, G. Adamkiewicz, J.D. Spengler, Quantifying the impact of traffic-related air pollution on the indoor air quality of a naturally ventilated building, *Environ. Int.* 89 (2016) 138–146, <https://doi.org/10.1016/j.envint.2016.01.016>.
- [25] F. Yang, Y. Kang, Y. Gao, K. Zhong, Numerical simulations of the effect of outdoor pollutants on indoor air quality of buildings next to a street canyon, *Build. Environ.* 87 (2015) 10–22, <https://doi.org/10.1016/j.buildenv.2015.01.008>.
- [26] M. Mohammadi, J. Calautit, Impact of ventilation strategy on the transmission of outdoor pollutants into indoor environment using CFD, *Sustainability* 13 (18) (2021) 10343, <https://doi.org/10.3390/su131810343>.
- [27] Y. Xiong, H. Chen, Effects of sunshields on vehicular pollutant dispersion and indoor air quality: Comparison between isothermal and nonisothermal conditions, *Build. Environ.* 197 (2021) 107854, <https://doi.org/10.1016/j.buildenv.2021.107854>.
- [28] F. Allard, M. Santamouris, S. Alvarez, European Commission Directorate-General for Energy & ALTENER Programme, in: *Natural ventilation in buildings: a design handbook*, James and James (Science Publishers), 1998. ISBN: 978-18-739-3672-6.
- [29] H.Y. Zhong, Y. Sun, J. Shang, F.P. Qian, F.Y. Zhao, H. Kikumoto, X. Liu, Single-sided natural ventilation in buildings: a critical literature review, *Build. Environ.* 212 (2022) 108797, <https://doi.org/10.1016/j.buildenv.2022.108797>.
- [30] Y. Hu, Y. Wu, Q. Wang, J. Hang, Q. Li, J. Liang, H. Ling, X. Zhang, Impact of indoor-outdoor temperature difference on building ventilation and pollutant dispersion within urban communities, *Atmosphere* 13 (1) (2021) 28, <https://doi.org/10.3390/atmos13010028>.
- [31] Z.T. Ai, C.M. Mak, From street canyon microclimate to indoor environmental quality in naturally ventilated urban buildings: Issues and possibilities for improvement, *Build. Environ.* 94 (2015) 489–503, <https://doi.org/10.1016/j.buildenv.2015.10.008>.
- [32] J.L. Santiago, E. Rivas, B. Sanchez, R. Buccolieri, F. Martín, The impact of planting trees on NO_x concentrations: The case of the Plaza de la Cruz neighborhood in Pamplona (Spain), *Atmosphere* 8 (7) (2017) 131, <https://doi.org/10.3390/atmos8070131>.
- [33] A. Martilli, B. Sánchez, J.L. Santiago, D. Rasilla, G. Pappacogli, F. Allende, F. Martín, C. Román-Cascón, C. Yagüe, F. Fernández, Simulating the pollutant dispersion during persistent wintertime thermal inversions over urban areas. The case of Madrid, *Atmos. Res.* 270 (2022) 106058, <https://doi.org/10.1016/j.atmosres.2022.106058>.
- [34] E. Alonso-Blanco, F.J. Gómez-Moreno, E. Díaz-Ramiro, J. Fernández, E. Coz, C. Yagüe, C. Román-Cascón, R. Borge, A. Narros, B. Artíñano, Real-Time Measurements of Indoor–Outdoor Exchange of Gaseous and Particulate Atmospheric Pollutants in an Urban Area, *Int. J. Environ. Res. Publ. Health* 20 (19) (2023) 6823, <https://doi.org/10.3390/ijerph20196823>.
- [35] R. Borge, J.L. Santiago, D. de la Paz, F. Martín, J. Domingo, C. Valdés, B. Sánchez, E. Rivas, Rozas, T. Ma, S. Lázaro, J. Pérez, Á. Fernández, Application of a short term air quality action plan in Madrid (Spain) under a high-pollution episode-Part II: Assessment from multi-scale modelling, *Sci. Total Environ.* 635 (2018) 1574–1584, <https://doi.org/10.1016/j.scitotenv.2018.04.323>.
- [36] L. Ntziachristos, D. Gkatzoflias, C. Kouridis, Z. Samaras, COPERT: a European road transport emission inventory model, in: *Information Technologies in Environmental Engineering: Proceedings of the 4th International ICSC Symposium.*, Springer Berlin Heidelberg, Thessaloniki, Greece, 2009, pp. 491–504, https://doi.org/10.1007/978-3-540-88351-7_37. May 28–29, 2009.
- [37] J. Pérez, J.M. de Andrés, R. Borge, D. de la Paz, J. Lumbreras, E. Rodríguez, Vehicle fleet characterization study in the city of Madrid and its application as a support tool in urban transport and air quality policy development, *Transport Pol.* 74 (2019) 114–126, <https://doi.org/10.1016/j.tranpol.2018.12.002>.
- [38] M. Pujadas, L. Nunez, J. Plaza, J.C. Bezares, J.M. Fernandez, Comparison between experimental and calculated vehicle idle emission factors for Madrid fleet, *Sci. Total Environ.* 334 (2004) 133–140, <https://doi.org/10.1016/j.scitotenv.2004.04.033>.
- [39] B. Das, P.V. Bhavne, S.P. Puppala, S. Adhikari, S. Sainju, E. Mool, R.M. Byanju, Emission factors and emission inventory of diesel vehicles in Nepal, *Sci. Total Environ.* 812 (2022) 152539, <https://doi.org/10.1016/j.scitotenv.2021.152539>.
- [40] J. Franke, A. Hellsten, K.H. Schlunzen, B. Carissimo, The COST 732 Best Practice Guideline for CFD simulation of flows in the urban environment: a summary, *Int. J. Environ. Pollut.* 44 (1–4) (2011) 419–427, <https://doi.org/10.1504/IJEP.2011.038443>.
- [41] S.D. Sabatino, R. Buccolieri, H.R. Olesen, M. Ketzler, R. Berkowicz, J. Franke, et al., COST 732 in practice: the MUST model evaluation exercise, *Int. J. Environ. Pollut.* 44 (1–4) (2011) 403–418, <https://doi.org/10.1504/IJEP.2011.038442>.
- [42] Siemens Digital Industries, *Simcenter STAR-CCM+ software*, Software (2023). <https://plm.sw.siemens.com/es-ES/simcenter/fluids-thermal-simulation/star-ccm/>.
- [43] H.K. Versteeg, W. Malalasekera. *An introduction to computational fluid dynamics: the finite volume method*, 2nd Ed., Pearson Education, 2007, ISBN 978-01-312-7498-3.
- [44] R. Ramponi, B. Blocken, CFD simulation of cross-ventilation for a generic isolated building: impact of computational parameters, *Build. Environ.* 53 (2012) 34–48, <https://doi.org/10.1016/j.buildenv.2012.01.004>.
- [45] D.B. Spalding, Mixing and chemical reaction in steady confined turbulent flames, *Symp. (Int.) Combust.* 13 (1) (1971) 649–657, [https://doi.org/10.1016/S0082-0784\(71\)80067-X](https://doi.org/10.1016/S0082-0784(71)80067-X).
- [46] Y. Li, T. Stathopoulos, Numerical evaluation of wind-induced dispersion of pollutants around a building, *J. Wind Eng. Ind. Aerod.* 67 (1997) 757–766, [https://doi.org/10.1016/S0167-6105\(97\)00116-5](https://doi.org/10.1016/S0167-6105(97)00116-5).

- [47] X. Wang, K.F. McNamara, Evaluation of CFD simulation using RANS turbulence models for building effects on pollutant dispersion, *Environ. Fluid Mech.* 6 (2006) 181–202, <https://doi.org/10.1007/s10652-005-5656-9>.
- [48] P.J. Richards, R.P. Hoxey, Appropriate boundary conditions for computational wind engineering models using the k- ϵ turbulence model, *J. Wind Eng. Ind. Aerod.* 46 (1993) 145–153, [https://doi.org/10.1016/0167-6105\(93\)90124-7](https://doi.org/10.1016/0167-6105(93)90124-7).
- [49] World Health Organization, Roadmap to Improve and Ensure Good Indoor Ventilation in the Context of COVID-19, Available at: <https://www.who.int/publications/i/item/9789240021280>, 2021.
- [50] E. Rivas, J.L. Santiago, F. Martín, A. Martilli, Impact of natural ventilation on exposure to SARS-CoV 2 in indoor/semi-indoor terraces using CO2 concentrations as a proxy, *J. Build. Eng.* 46 (2022) 103725, <https://doi.org/10.1016/j.jobte.2021.103725>.
- [51] N. Nikolopoulos, A. Nikolopoulos, T.S. Larsen, K.S.P. Nikas, Experimental and numerical investigation of the tracer gas methodology in the case of a naturally cross-ventilated building, *Build. Environ.* 56 (2012) 379–388, <https://doi.org/10.1016/j.buildenv.2012.04.006>.
- [52] D. Etheridge, *Natural ventilation of buildings: theory, measurement and design*, 1st Ed., Wiley, 2011, ISBN 9781119954378.
- [53] J. McWilliams, Review of air flow measurement techniques, Available at: <https://www.osti.gov/servlets/purl/809884>, 2002. DOI: 10.2172/809884.
- [54] Siemens Digital Industries Software, STAR-CCM+16.02.009-R8® User Guide, 2023.
- [55] C. Román-Cascón, A. Yagüe, J.A. Arrillaga, M. Lothon, E.R. Pardyjak, F. Lohou, I. Turki, Comparing mountain breezes and their impacts on CO₂ mixing ratios at three contrasting areas, *Atmos. Res.* 221 (2019) 111–126, <https://doi.org/10.1016/j.atmosres.2019.01.019>.
- [56] J.C. Chang, S.R. Hanna, Air quality model performance evaluation, *Meteorol. Atmos. Phys.* 87 (1–3) (2004) 167–196, <https://doi.org/10.1007/s00703-003-0070-7>.
- [57] J.L. Santiago, B. Sanchez, C. Quaassdorff, D. de la Paz, A. Martilli, F. Martín, R. Borge, E. Rivas, F.J. Gómez-Moreno, E. Díaz, B. Artífano, C. Yagüe, S. Vardoulakis, Performance evaluation of a multiscale modelling system applied to particulate matter dispersion in a real traffic hot spot in Madrid (Spain), *Atmos. Pollut. Res.* 11 (1) (2020) 141–155, <https://doi.org/10.1016/j.apr.2019.10.001>.
- [58] J.L. Santiago, B. Sanchez, E. Rivas, M.G. Vivanco, M.R. Theobald, J.L. Garrido, V. Gil, A. Martilli, A. Rodríguez-Sánchez, R. Buccolieri, F. Martín, High spatial resolution assessment of the effect of the Spanish National Air Pollution Control Programme on street-level NO₂ concentrations in three neighborhoods of Madrid (Spain) using mesoscale and CFD modelling, *Atmosphere* 13 (2) (2022) 248, <https://doi.org/10.3390/atmos13020248>.
- [59] C. Quaassdorff, R. Borge, J. Pérez, J. Lumbreras, D. de la Paz, J.M. de Andrés, Microscale traffic simulation and emission estimation in a heavily trafficked roundabout in Madrid (Spain), *Sci. Total Environ.* 566 (2016) 416–427, <https://doi.org/10.1016/j.scitotenv.2016.05.051>.
- [60] I. Castañeda Díez, Modelización CFD (Computational Fluid Dynamics) del intercambio de contaminantes entre los ambientes exterior e interior por ventilación natural en un entorno urbano, Master's thesis, Universidad Complutense de Madrid, 2023. Available at: <https://hdl.handle.net/20.500.14352/91383>.

Nomenclature

Acronyms

ACHs: Air Changes per Hour
 AGL: Above Ground Level
 AQMS: Air Quality Monitoring Stations
 CFD: Computational Fluid Dynamics
 CFL: Courant number
 EU: European Union
 HS: Heat source
 IAQ: Indoor Air Quality
 LES: Large Eddy Simulations
 LiDAR: Light Detection and Ranging
 LST: Local Solar Time
 PM: Particulate Matter
 PL: Prismatic Layer
 RE: Relative Error
 SS: Single-Sided
 URANS: Unsteady Reynolds-Averaged Navier-Stokes
 WHO: World Health Organization

Symbols

ΔS : Surface size (m²)
 Δt : Time-step (s)
 ΔV : Volume size (m³)
 ϵ : Turbulent dissipation rate (m² s⁻³)
 κ : Turbulent kinetic energy (J kg⁻¹)
 k : Von Karman's constant
 ρ : Density (kg m⁻³)
 μ_t : Turbulent dynamic viscosity (Pa s)
 τ : Characteristic time (s)
 A_C : Ambulance mass flow rate (g h⁻¹)
 C : Concentration (μ m⁻³)
 E_C : Road mass flow rate (g h⁻¹)
 I_C : Infiltration concentration (μ m⁻³)
 Q : Mass flux (kg m⁻² s⁻¹)
 \vec{r} : Position (m)
 Sc_t : Schmidt number
 t : Time (s)
 T : Temperature (K)
 u^* : Friction velocity (m s⁻¹)
 u_j : j-component of flow (m s⁻¹)
 UB_C : Urban background concentration (μ m⁻³)
 WS : Wind speed (m s⁻¹)
 WD : Wind direction (°)

(x, y, z) : Cartesian coordinates (m)

z_0 : Roughness (m)

Z : Height (m)

Subscripts

d: down

f: far

in: indoor

max: maximum

min: minimum

n: near

norm: normalized

out: outdoor

u: up